J. Fluid Mech. (2025), *vol.* 1009, A64, doi:10.1017/jfm.2025.303

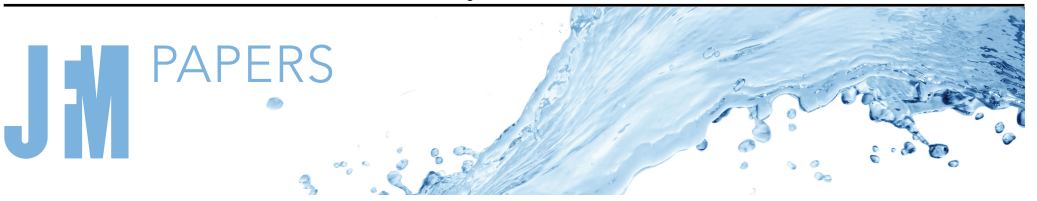

A three-dimensional long-wave steep-slope equation

Rafael Schwartz

Department of Civil Engineering, Ariel University, Ariel 40700, Israel

Corresponding author: Rafael Schwartz, rafaelsc@ariel.ac.il

(Received 27 October 2024; revised 4 March 2025; accepted 11 March 2025)

A complete three-dimensional long-wave polar–Cartesian equation is developed in the frequency domain. This development employs an auxiliary axis system oriented locally in the bottom gradient direction. The long-wave limit of the two-dimensional polar–Cartesian steep-slope equation is also derived. An approximate explicit expression of the coefficients is developed without restrictions on bed steepness. This is achieved by utilising a rational function approximation of the arctan function, which arises from the formulation of the vertical profile of the flow parameters. Additionally, long-wave equations in both two and three dimensions are developed in the time domain. Simulations of the long-wave equations are compared with those of the extended shallow-water equation for two-dimensional test cases, as well as for the quasi-three-dimensional scenario of oblique incidence. Our equations exhibit better agreement with the exact solutions in the majority of the test cases.

Key words: surface gravity waves

1. Introduction

Mild-slope equations (MSEs) are approximated models developed for free-surface wave propagation over mild slopes of the sea floor. Commonly, the vertical profile of the velocity field is approximated as the solution of time-harmonic, linear propagating waves over a horizontal bottom. Berkhoff (1972) introduced the MSE that accounts for the leading-order term in the bottom slope. Smith & Sprinks (1975) were the first to introduce the second-order terms, followed by several others (e.g. Kirby 1986; Chamberlain & Porter 1995). Miles & Chamberlain (1998) introduced the fourth-order terms.

Kim & Bai (2004) shifted the formulation from the potential to the stream function, providing a more accurate representation of the bottom boundary by defining it as a

© The Author(s), 2025. Published by Cambridge University Press. This is an Open Access article, distributed under the terms of the Creative Commons Attribution licence (https://creativecommons.org/licenses/by/4.0/), which permits unrestricted re-use, distribution and reproduction, provided the original article is properly cited.

https://doi.org/10.1017/jfm.2025.303 Published online by Cambridge University Press

streamline. The superior performance of this model is somewhat overshadowed by the vector equation which is derived for the three-dimensional (3-D) case. The drawback of dealing with a vector equation was overcome by Toledo & Agnon (2010) who formulated an equivalent scalar equation by introducing a pseudo-potential formulation.

In all of these equations, the flow problem was defined using the Cartesian coordinate system, where the most simplistic boundary shape is a rectangle. This incorporates a boundary on the linear free surface and on a horizontal bed, in addition to lateral boundary conditions. The vertical profiles are subsequently calculated as the solution of waves propagating over a horizontal bottom.

Belibassakis & Athanassoulis (2006) addressed normally incident waves on a sloping plane beach using polar coordinates. A polar MSE provides an accurate representation of flow problems with radial-shaped bathymetries. The use of polar coordinates, as opposed to Cartesian coordinates, introduces a bathymetry with a constant-slope bed as the basic problem formulation. Therefore, the vertical profiles arising from the polar formulation include the bottom gradient, which is absent from the Cartesian-based profiles. This led Schwartz *et al.* (2023) to formulate the polar–Cartesian (PC) MSE (PCMSE) by introducing the Cartesian equivalent of the polar vertical profile. This approach utilises the advantage of each coordinate system: on the one hand, it introduces a more accurate vertical profile than the Cartesian-based equations and, on the other hand, it provides satisfactory results for non-radial problems. The analytical formulation of the coefficients in the resulting equation was lengthy and complex, resolved by a series expansion in the bottom steepness. Alternatively, the coefficients were calculated numerically, in which case there are no limitations on the bottom slope. The equation is therefore also referred to as the PC steep-slope equation (PCSSE).

A two-dimensional (2-D) long-wave limit of this equation, referred to as the long PC steep-slope equation (LPCSSE), is developed in § 2. In this equation, an analytical approximation of the coefficients is provided without limitations regarding the bottom slope. In § 3, a long-wave 3-D PC equation is developed, complementing the 2-D and quasi-3-D equations developed in Schwartz *et al.* (2023). In the PCSSE, the velocity profiles are influenced by the wavenumbers in the x and y directions, which in turn are dependent on the wave direction. This dependency creates a challenge in formulating a general 3-D equation. However, when considering the long-wave limit, the velocity profiles are independent of the wavenumber, facilitating the development of a 3-D equation for this case. In § 4, 2-D and 3-D long-wave PC equations are developed in the time domain. These equations are referred to as the long time-dependent PC equations (LTDPCEs). This is accomplished by following the procedure presented in Porter (2019) which extended the shallow-water equation to the next order. The equation provided there is referred to as the extended shallow-water equation (ESWE) and is effectively a long-wave limit of the complementary MSE. As stated in that work, the validity of such linear long-wave-limit equations is ensured by assuming that the free-surface elevation, ζ, remains small, with $|\nabla\zeta| \approx (|\zeta|/\lambda) \ll ((h/\lambda))^3$, where h denotes the depth and λ the wavelength. Simulations of the 2-D LPCSSE and LTDPCE are presented in § 5 and compared with the ESWE. In § 6, conclusions are drawn.

2. The 2-D long-wave PCSSE

The equations governing the irrotational flow of an incompressible, inviscid fluid with a free surface, in terms of the polar coordinates, are given by

$$\frac{1}{r}\frac{\partial}{\partial r}\left(r\frac{\partial \psi}{\partial r}\right)+\frac{1}{r^2}\frac{\partial^2 \psi}{\partial \theta^2}=0, \quad -\alpha<\theta<0, \tag{2.1}$$

https://doi.org/10.1017/jfm.2025.303 Published online by Cambridge University Press

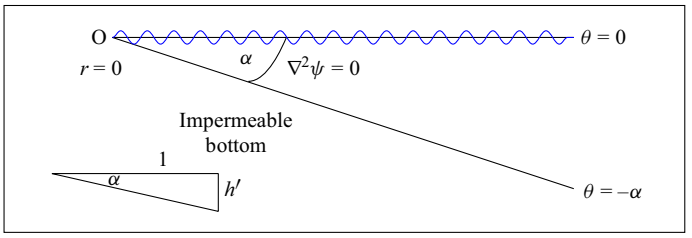

Figure 1. Polar coordinates: problem description.

$$\frac{1}{r}\frac{\partial \psi}{\partial \theta} + \frac{1}{\sigma}\frac{\partial^2 \psi}{\partial r^2} = 0, \quad \theta = 0, \tag{2.2}$$

$$\psi = 0, \quad \theta = -\alpha, \tag{2.3}$$

where r and θ are the radial distance and angle, respectively, $\theta = 0$ represents the mean free surface, $\theta = -\alpha$ the bottom location and $r = 0$ the shore, as depicted in figure 1. This formulation refers to a time-harmonic flow such that the time-harmonic stream function is defined by $\mathrm{Re}[\psi \mathrm{e}^{-\mathrm{i}\omega t}]$, where ω is the angular frequency of the incoming wave and $\sigma = \omega^2/g$, g being the gravitational acceleration. Function $\psi = \psi(r, \theta)$ is a complex-valued function.

Schwartz *et al.* (2023) derived the PCSSE using the following normalised, θ-dependent profile:

$$F_p(\theta) = \frac{\sinh(\gamma(\theta + \alpha))}{\sinh(\gamma\alpha)}, \tag{2.4}$$

where γ is a constant, equivalent to the wavenumber in the Cartesian formulation. The vertical analytical integration of the Cartesian-equivalent profile produced complex terms, necessitating the numerical calculation of the coefficients. In the following, we consider the long-wave limit of this profile, which significantly simplifies the coefficients and enables the use of analytical expressions based on this approximation. This is achieved by taking the leading-order term of the polar profile for a long-wave approximation ($\gamma\theta, \gamma\alpha \ll 1$) (2.4):

$$F_p(\theta) \approx 1 + \frac{\theta}{\alpha} + O\left((\gamma\alpha)^3\right). \tag{2.5}$$

The equivalent Cartesian terms are derived by substituting the following relations (figure 2):

$$\theta = \arctan\left(\frac{zh'}{h}\right), \quad \alpha = \arctan(h'). \tag{2.6}$$

Here h' is the slope of the bottom bathymetry and is defined in figure 1. The vertical Cartesian-equivalent profile, neglecting the higher-order terms, is given as

$$F_{pc}\left(h(x), h'(x), z\right) = 1 + \frac{\arctan\left(zh'/h\right)}{\arctan(h')}. \tag{2.7}$$

The vertical integration of this simplified profile still presents some complications. Integrating $\arctan(n)$ with respect to a general parameter n leads to expressions involving non-elementary functions. To avoid these terms and simplify the mathematical representation of the coefficients, we utilise an approximation of this function, as provided

https://doi.org/10.1017/jfm.2025.303 Published online by Cambridge University Press

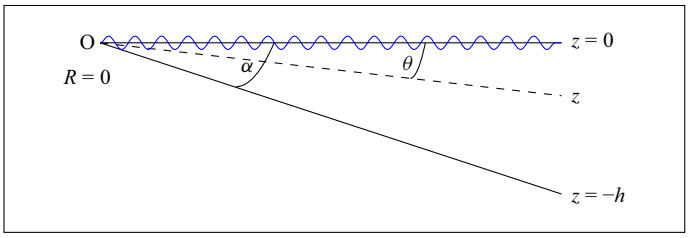

Figure 2. Polar–Cartesian relations.

in Hastings (1955). This approximation is represented as a polynomial of n and has a maximum error of 0.6 per mil in the range $|\,n\,| \leq 1$:

$$App_1: \quad \arctan(n) \approx c_1 n + c_3 n^3 + c_5 n^5, \tag{2.8}$$

with $c_1 = 0.995354$, $c_3 = -0.288679$ and $c_5 = 0.079331$. In the rest of the region, a similar approximation for the inverse parameter $1/n$ can be utilised, providing a rational function approximation:

$$App_2: \quad \arctan(n) \approx \frac{Pi}{2} - \left(c_1 \frac{1}{n} + c_3 \frac{1}{n^3} + c_5 \frac{1}{n^5}\right) \quad \text{in } n > 1, \tag{2.9}$$

$$App_3: \quad \arctan(n) \approx -\frac{Pi}{2} - \left(c_1 \frac{1}{n} + c_3 \frac{1}{n^3} + c_5 \frac{1}{n^5}\right) \quad \text{in } n < -1 \tag{2.10}$$

with the same maximum error.

Noting that $(z/h) \leq 1$, the term in the numerator of (2.7), (zh'/h), can be classified by dividing it into three regions:

(i) $|\,h'\,| \leq 1$. The absolute value of the integrand is smaller than that along the integration range, and therefore: $\int_{-h}^{0} F\,\mathrm{d}z = \int_{-h}^{0} App_1\,\mathrm{d}z$.

(ii) $h' > 1$. The integrand crosses two approximation regions, and therefore the integration is divided into two parts: $\int_{-h}^{0} F\,\mathrm{d}z = \int_{-h}^{-h/h'} App_3\,\mathrm{d}z + \int_{-h/h'}^{0} App_1\,\mathrm{d}z$.

(iii) $h' < -1$. The approximation is also divided into two parts: $\int_{-h}^{0} F\,\mathrm{d}z = \int_{-h}^{h/h'} App_2\,\mathrm{d}z + \int_{h/h'}^{0} App_1\,\mathrm{d}z$.

Applying this approximation requires distinguishing between the different regions of the bottom slope along the flow. Once the region is identified, the appropriate integrand can be substituted. An additional option is to numerically integrate the vertical profile. In both options, there are no limitations on the steepness of the bottom slope, leading to a 2-D steep-slope equation, referred to as the LPCSSE.

3. The 3-D PCSSE

The challenge in deriving an equation for a 3-D geometry stems from the varying direction of the depth gradient at each location. In addition, the wavenumber components in the x and y directions are influenced by the depth gradient direction, necessitating their determination at each point. By taking the long-wave limit, the velocity profiles become independent of the wavenumber, helping to overcome this challenge. The remaining issue is addressed by defining a local axis system where the x axis is aligned with the depth

https://doi.org/10.1017/jfm.2025.303 Published online by Cambridge University Press

gradient direction at each point and the y axis is perpendicular to the x axis. This results in a locally horizontal depth in the direction of y.

The time-harmonic vector stream function is defined as

$$\boldsymbol{\Psi}(x, y, z) = (f_1\psi_1(x, y),\ f_2\psi_2(x, y)). \tag{3.1}$$

The vertical profiles of the vector stream function are defined by

$$f_1(h, h', z) = \frac{\sinh\left(\gamma\left(\arctan(zh'/h) + \arctan(h')\right)\right)}{\sinh\left(\gamma\ \arctan(h')\right)}, \tag{3.2}$$

$$f_2(h, z) = \frac{\sinh\left(k(z+h)\right)}{\sinh(kh)}, \tag{3.3}$$

where γ is the x component and k is the y component of the wavenumber vector, f_1 is the Cartesian equivalent of the polar profile and f_2 corresponds to a horizontal bottom.

The velocities are calculated accordingly:

$$\mathbf{u}(x, y, z) = (u(x, y, z),\ v(x, y, z)) = \left(f_{1_z}\psi_1,\ f_{2_z}\psi_2\right), \tag{3.4}$$

$$w(x, y, z) = -\nabla\cdot\boldsymbol{\Psi} = -f_{1_x}\psi_1 - f_1\psi_{1_x} - f_2\psi_{2_y}, \tag{3.5}$$

where $\nabla = (\partial_x, \partial_y)$.

The free-surface location is derived from the linear kinematic condition:

$$\eta(x, y) = \frac{1}{\mathrm{i}\omega}\nabla\cdot\Psi_0(x, y) = \frac{1}{\mathrm{i}\omega}\left(\psi_{1_x}(x, y) + \psi_{2_y}(x, y)\right). \tag{3.6}$$

These terms are substituted into the time-averaged Lagrangian density:

$$\begin{aligned} L &= \int_{-h}^{0}\left(|u|^2 + |v|^2 + |w|^2\right)\mathrm{d}z - g|\eta|^2 \\ &= d_1|\psi_1|^2 + d_2|\psi_2|^2 + c|\psi_1|^2 + a_1|\psi_{1_x}|^2 + a_2|\psi_{2_y}|^2 \\ &\quad + 2b_1\mathrm{Re}(\psi_1\psi_{1_x}*) + 2b_2\mathrm{Re}(\psi_1\psi_{2_y}*) + 2e\mathrm{Re}(\psi_{1_x}\psi_{2_y}*), \end{aligned} \tag{3.7}$$

where the coefficients are defined as

$$a_1 = \int f_1^2\,\mathrm{d}z - \frac{1}{\sigma}, \quad a_2 = \int f_2^2\,\mathrm{d}z - \frac{1}{\sigma}, \quad b_1 = \int f_1 f_{1_x}\,\mathrm{d}z, \quad b_2 = \int f_2 f_{1_x}\,\mathrm{d}z, \tag{3.8}$$

$$c = \int f_{1_x}^2\,\mathrm{d}z, \quad e = \int f_1 f_2\,\mathrm{d}z - \frac{1}{\sigma}, \quad d_1 = \int f_{1_z}^2\,\mathrm{d}z, \quad d_2 = \int f_{2_z}^2\,\mathrm{d}z. \tag{3.9}$$

The variation with respect to ψ_1 results in

$$\frac{\delta L}{\delta\psi_1} = \frac{\partial L}{\partial\psi_1} - \frac{\partial}{\partial x}\frac{\partial L}{\partial\psi_{1_x}} = 0,$$

$$a_1\psi_{1_{xx}} + e\psi_{2_{xy}} + a_{1_x}\psi_{1_x} + (e_x - b_2)\psi_{2_y} + (b_{1_x} - c - d_1)\psi_1 = 0. \tag{3.10}$$

The variation with respect to ψ_2 provides the coupled equation

$$\frac{\delta L}{\delta\psi_2} = \frac{\partial L}{\partial\psi_2} - \frac{\partial}{\partial y}\frac{\partial L}{\partial\psi_{2_y}} = 0,$$

$$a_2\psi_{2_{yy}} + e\psi_{1_{xy}} + b_2\psi_{1_y} - d_2\psi_2 = 0. \tag{3.11}$$

Equations (3.10) and (3.11) constitute a coupled system on the dynamic x, y axes. The equations are now rotated to the static axis system for which $\tilde{x}$ is perpendicular and $\tilde{y}$ is

https://doi.org/10.1017/jfm.2025.303 Published online by Cambridge University Press

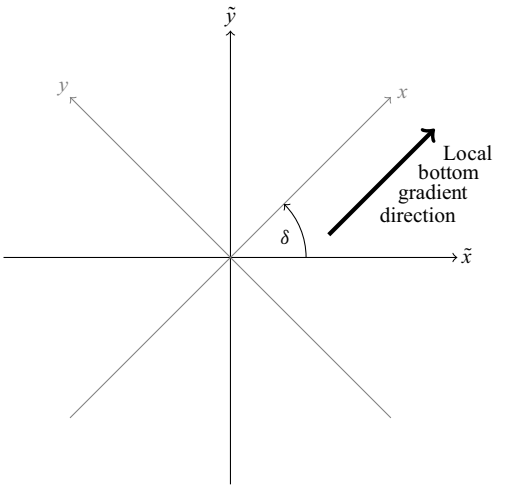

Figure 3. The dynamic x, y and static $\tilde{x}$, $\tilde{y}$ Cartesian axis systems. The x axis is aligned with the direction of the local bottom gradient. The z and $\tilde{z}$ axes are parallel to the drawing plane. Angle δ represents the counterclockwise angle between the two axis systems.

parallel to the shoreline. Defining δ as the counterclockwise rotation angle between the two systems (figure 3), we can define

$$\tilde{x} = x\cos\delta - y\sin\delta, \tag{3.12}$$
$$\tilde{y} = x\sin\delta + y\cos\delta. \tag{3.13}$$

The relationships between the derivatives in the $(\tilde{x}, \tilde{y})$ and (x, y) coordinate systems are given by

$$\psi_y = -\sin(\delta)\tilde{\psi}_{\tilde{x}} + \cos(\delta)\tilde{\psi}_{\tilde{y}}, \tag{3.14}$$
$$\psi_{yy} = \sin^2(\delta)\tilde{\psi}_{\tilde{x}\tilde{x}} - \sin(2\delta)\tilde{\psi}_{\tilde{x}\tilde{y}} + \cos^2(\delta)\tilde{\psi}_{\tilde{y}\tilde{y}}, \tag{3.15}$$
$$\psi_x = \cos(\delta)\tilde{\psi}_{\tilde{x}} + \sin(\delta)\tilde{\psi}_{\tilde{y}}, \tag{3.16}$$
$$\psi_{xx} = \cos^2(\delta)\tilde{\psi}_{\tilde{x}\tilde{x}} + \sin(2\delta)\tilde{\psi}_{\tilde{x}\tilde{y}} + \sin^2(\delta)\tilde{\psi}_{\tilde{y}\tilde{y}}, \tag{3.17}$$
$$\psi_{xy} = \frac{\sin(2\delta)}{2}(\tilde{\psi}_{\tilde{y}\tilde{y}} - \tilde{\psi}_{\tilde{x}\tilde{x}}) + \left(\cos^2(\delta) - \sin^2(\delta)\right)\tilde{\psi}_{\tilde{x}\tilde{y}}. \tag{3.18}$$

Additionally, the relationships between the coefficients are given by

$$b_1 = \cos(\delta)\widetilde{bx}_1 + \sin(\delta)\widetilde{by}_1, \quad b_2 = \cos(\delta)\widetilde{bx}_2 + \sin(\delta)\widetilde{by}_2, \tag{3.19}$$
$$c = \cos^2(\delta)\widetilde{cx} + \sin(2\delta)\widetilde{cxy} + \sin^2(\delta)\widetilde{cy}, \tag{3.20}$$

where

$$\widetilde{bx}_1 = \int \tilde{f}_1\tilde{f}_{1_{\tilde{x}}}\,\mathrm{d}z, \quad \widetilde{by}_1 = \int \tilde{f}_1\tilde{f}_{1_{\tilde{y}}}\,\mathrm{d}z, \quad \widetilde{bx}_2 = \int \tilde{f}_2\tilde{f}_{1_{\tilde{x}}}\,\mathrm{d}z, \quad \widetilde{by}_2 = \int \tilde{f}_2\tilde{f}_{1_{\tilde{y}}}\,\mathrm{d}z, \tag{3.21}$$

$$\widetilde{cx} = \int \tilde{f}_{1_{\tilde{x}}}^2\,\mathrm{d}z, \quad \widetilde{cxy} = \int \tilde{f}_{1_{\tilde{x}}}\tilde{f}_{1_{\tilde{y}}}\,\mathrm{d}z, \quad \widetilde{cy} = \int \tilde{f}_{1_{\tilde{y}}}^2\,\mathrm{d}z. \tag{3.22}$$

https://doi.org/10.1017/jfm.2025.303 Published online by Cambridge University Press

Equations (3.10) and (3.11) are now expressed in the static coordinate system. The transformed form of equation (3.10) is given by

$$\begin{aligned}
&\tilde{a}_1\left(\cos^2(\delta)\tilde{\psi}_{1_{\tilde{x}\tilde{x}}}+\sin(2\delta)\tilde{\psi}_{1_{\tilde{x}\tilde{y}}}+\sin^2(\delta)\tilde{\psi}_{1_{\tilde{y}\tilde{y}}}\right)\\
&\quad+\tilde{e}\left(\frac{1}{2}\sin(2\delta)(\tilde{\psi}_{2_{\tilde{y}\tilde{y}}}-\tilde{\psi}_{2_{\tilde{x}\tilde{x}}})+(\cos^2(\delta)-\sin^2(\delta))\tilde{\psi}_{2_{\tilde{x}\tilde{y}}}\right)\\
&\quad+\left(\cos(\delta)\tilde{a}_{1_{\tilde{x}}}+\sin(\delta)\tilde{a}_{1_{\tilde{y}}}\right)\left(\cos(\delta)\tilde{\psi}_{1_{\tilde{x}}}+\sin(\delta)\tilde{\psi}_{1_{\tilde{y}}}\right)\\
&\quad+\left(\cos(\delta)\tilde{e}_{\tilde{x}}+\sin(\delta)\tilde{e}_{\tilde{y}}-\cos(\delta)\widetilde{bx}_2-\sin(\delta)\widetilde{by}_2\right)\left(\cos(\delta)\tilde{\psi}_{2_{\tilde{y}}}-\sin(\delta)\tilde{\psi}_{2_{\tilde{x}}}\right)\\
&\quad+\left(\cos^2(\delta)\widetilde{bx}_{1_{\tilde{x}}}+\frac{1}{2}\sin(2\delta)\widetilde{by}_{1_{\tilde{x}}}+\frac{1}{2}\sin(2\delta)\widetilde{bx}_{1_{\tilde{y}}}+\sin^2(\delta)\widetilde{by}_{1_{\tilde{y}}}\right.\\
&\quad\left.-\cos^2(\delta)\tilde{c}_{\tilde{x}}-\sin(2\delta)\tilde{c}_{\tilde{x}\tilde{y}}-\sin^2(\delta)\tilde{c}_{\tilde{y}}-\tilde{d}_1\right)\tilde{\psi}_1=0.
\end{aligned}\tag{3.23}$$

Similarly, the transformed form of equation (3.11) is given by

$$\begin{aligned}
&\tilde{a}_2\left(\sin^2(\delta)\tilde{\psi}_{2_{\tilde{x}\tilde{x}}}-\sin(2\delta)\tilde{\psi}_{2_{\tilde{x}\tilde{y}}}+\cos^2(\delta)\tilde{\psi}_{2_{\tilde{y}\tilde{y}}}\right)\\
&\quad+\tilde{e}\left(\frac{1}{2}\sin(2\delta)(\tilde{\psi}_{1_{\tilde{x}\tilde{y}}}-\tilde{\psi}_{1_{\tilde{x}\tilde{x}}})+(\cos^2(\delta)-\sin^2(\delta))\tilde{\psi}_{1_{\tilde{x}\tilde{y}}}\right)\\
&\quad+\left(\cos(\delta)\widetilde{bx}_2+\sin(\delta)\widetilde{by}_2\right)\left(\tilde{\psi}_{1_{\tilde{y}}}\cos(\delta)-\tilde{\psi}_{1_{\tilde{x}}}\sin(\delta)\right)-\tilde{d}_2\tilde{\psi}_2=0.
\end{aligned}\tag{3.24}$$

Dividing both equations by $\cos^2(\delta)$ provides

$$\begin{aligned}
&\tilde{a}_1\left(\tilde{\psi}_{1_{\tilde{x}\tilde{x}}}+2\tan(\delta)\tilde{\psi}_{1_{\tilde{x}\tilde{y}}}+\tan^2(\delta)\tilde{\psi}_{1_{\tilde{y}\tilde{y}}}\right)\\
&\quad+\tilde{e}\left(\tan(\delta)(\tilde{\psi}_{2_{\tilde{y}\tilde{y}}}-\tilde{\psi}_{2_{\tilde{x}\tilde{x}}})+(1-\tan^2(\delta))\tilde{\psi}_{2_{\tilde{x}\tilde{y}}}\right)\\
&\quad+\left(\tilde{a}_{1_{\tilde{x}}}+\tan(\delta)\tilde{a}_{1_{\tilde{y}}}\right)\left(\tilde{\psi}_{1_{\tilde{x}}}+\tan(\delta)\tilde{\psi}_{1_{\tilde{y}}}\right)\\
&\quad+\left(\tilde{e}_{\tilde{x}}+\tan(\delta)\tilde{e}_{\tilde{y}}-\widetilde{bx}_2-\tan(\delta)\widetilde{by}_2\right)\left(\tilde{\psi}_{2_{\tilde{y}}}-\tan(\delta)\tilde{\psi}_{2_{\tilde{x}}}\right)\\
&\quad+\left(\widetilde{bx}_{1_{\tilde{x}}}+\tan(\delta)\widetilde{by}_{1_{\tilde{x}}}+\tan(\delta)\widetilde{bx}_{1_{\tilde{y}}}+\tan^2(\delta)\widetilde{by}_{1_{\tilde{y}}}\right.\\
&\quad\left.-\tilde{c}_{\tilde{x}}-2\tan(\delta)\tilde{c}_{\tilde{x}\tilde{y}}-\tan^2(\delta)\tilde{c}_{\tilde{y}}-\frac{\tilde{d}_1}{\tan^2(\delta)}\right)\tilde{\psi}_1=0,
\end{aligned}\tag{3.25}$$

$$\begin{aligned}
&\tilde{a}_2\left(\tan^2(\delta)\tilde{\psi}_{2_{\tilde{x}\tilde{x}}}-2\tan(\delta)\tilde{\psi}_{2_{\tilde{x}\tilde{y}}}+\tilde{\psi}_{2_{\tilde{y}\tilde{y}}}\right)\\
&\quad+\tilde{e}\left(\tan(\delta)(\tilde{\psi}_{1_{\tilde{x}\tilde{y}}}-\tilde{\psi}_{1_{\tilde{x}\tilde{x}}})+(1-\tan^2(\delta))\tilde{\psi}_{1_{\tilde{x}\tilde{y}}}\right)\\
&\quad+\left(\widetilde{bx}_2+\tan(\delta)\widetilde{by}_2\right)\left(\tilde{\psi}_{1_{\tilde{y}}}-\tan(\delta)\tilde{\psi}_{1_{\tilde{x}}}\right)-\frac{\tilde{d}_2}{\cos^2(\delta)}\tilde{\psi}_2=0.
\end{aligned}\tag{3.26}$$

Equations (3.10) and (3.11) are to be solved in the dynamic x, y, z coordinate system with the appropriate lateral boundary conditions. Following this, the system is rotated at each point by the rotation angle δ, as outlined in equations (3.12) and (3.13). Alternatively, equations (3.25) and (3.26) can be solved along with the rotated lateral boundary conditions.

https://doi.org/10.1017/jfm.2025.303 Published online by Cambridge University Press

4. The time-domain equation

Generally, mild-slope-type equations are time-harmonic, meaning they are defined in the frequency domain. Porter (2019) developed an ESWE by accounting for the next order in the wavelength. Following a similar procedure and using the PC vertical profiles, a MSE is formulated in the time domain. The 2-D case is addressed in § 4.1, while the 3-D case is covered in § 4.2.

4.1. *The 2-D equation*

The horizontal velocity is defined by a separation of variables:

$$u(x,z,t) = f_{1_z}(z,h(x),h'(x))u_0(x,t), \tag{4.1}$$

where f_1 is the vertical profile as calculated in equation (3.2).

Integrating vertically provides the stream function

$$\psi(x,z,t) = f_1 u_0, \tag{4.2}$$

and taking the horizontal derivative provides the vertical velocity component

$$w(x,z,t) = -f_{1_x}u_0 + f_1\zeta_t, \tag{4.3}$$

where the linear kinematic free-surface condition, $u_{0_x} = -\zeta_t$, was substituted. Here, $\zeta(x,t) = \eta(x)\mathrm{e}^{-\mathrm{i}\omega t}$.

It is noted that the bottom boundary condition, $w + h'u = 0$ on $z = -h$, is satisfied under this representation. This is in addition to the continuity equation, which is inherently satisfied by the stream function definition.

Next, the horizontal component of the linearised momentum equation is utilised:

$$\rho w_t = -p_z - \rho g, \tag{4.4}$$

and by substituting the vertical velocity profile, we derive

$$p_z = \rho\left(f_{1_x}u_{0_t} - f_1\zeta_{tt} - g\right), \tag{4.5}$$

where p denotes the pressure and ρ the fluid density.

The equation is vertically integrated from an arbitrary elevation, z, to the free surface, retaining only the leading-order terms:

$$p\,|_z^\zeta = p_a - p(z) = \rho\left(\left(\int_z^0 f_{1_x}\mathrm{d}z\right)u_{0_t} - \left(\int_z^0 f_1\mathrm{d}z\right)\zeta_{tt} - g(\zeta - z)\right), \tag{4.6}$$

after which the pressure is isolated:

$$p(z) = p_a + \rho\left(g(\zeta - z) - \left(\int_z^0 f_{1_x}\mathrm{d}z\right)u_{0_t} + \left(\int_z^0 f_1\mathrm{d}z\right)\zeta_{tt}\right). \tag{4.7}$$

Taking the derivative in the x direction:

$$\begin{aligned} p_x = \rho\Bigg(g\zeta_x - \left(\int_z^0 f_{1_x}\mathrm{d}z\right)_x u_{0_t} - \left(\int_z^0 f_{1_x}\mathrm{d}z\right)u_{0_{xt}} + \left(\int_z^0 f_1\mathrm{d}z\right)_x \zeta_{tt} \\ + \left(\int_z^0 f_1\mathrm{d}z\right)\zeta_{ttx}\Bigg). \end{aligned} \tag{4.8}$$

https://doi.org/10.1017/jfm.2025.303 Published online by Cambridge University Press

Defining $e = \int_z^0 f \, \mathrm{d}z$, the Leibniz integration rule is utilised to derive

$$p_x = \rho \left(g\zeta_x - e_{xx} u_{0_t} - e_x u_{0_{xt}} + e_x \zeta_{tt} + e\zeta_{ttx} \right). \tag{4.9}$$

This expression is substituted into the horizontal component of the momentum equation, applied in a vertically averaged sense:

$$\int_{-h}^{0} u_t \, \mathrm{d}z = -\frac{1}{\rho} \int_{-h}^{0} p_x \, \mathrm{d}z, \tag{4.10}$$

$$(1 - E_2)) \, u_{0_t} = -gh\zeta_x - 2E_1\zeta_{tt} - E_0\zeta_{ttx}, \tag{4.11}$$

where $E_0 = \int_{-h}^{0} e \, \mathrm{d}z$, $E_1 = \int_{-h}^{0} e_x \, \mathrm{d}z$ and $E_2 = \int_{-h}^{0} e_{xx} \, \mathrm{d}z$.

We then divide by the left-hand coefficient and differentiate with respect to x:

$$u_{0_{xt}} = -\frac{\partial}{\partial x} \left(\frac{gh\zeta_x + 2E_1\zeta_{tt} + E_0\zeta_{ttx}}{1 - E_2} \right). \tag{4.12}$$

The linear relation $u_{0_{xt}} = -\zeta_{tt}$ is utilised to eliminate u_0 and provide an equation as a function of ζ:

$$\zeta_{tt} = \frac{\partial}{\partial x} \left(\frac{gh\zeta_x + 2E_1\zeta_{tt} + E_0\zeta_{ttx}}{1 - E_2} \right). \tag{4.13}$$

This equation is referred to as the LTDPCE in the following sections.

4.2. *The 3-D equation*

The same procedure is applied here to the 3-D case. As in the equation in the frequency domain, a local axis system is oriented such that the x axis is aligned with the bottom gradient and perpendicular to the y axis. The same profiles are utilised:

$$\begin{aligned} \mathbf{u}(x, y, z, t) &= (u(x, y, z, t), v(x, y, z, t)) \\ &= \left(f_{1_z}(h, h', z) u_0(x, y, t), f_{2_z}(h, h', z) v_0(x, y, t) \right), \end{aligned} \tag{4.14}$$

$$\boldsymbol{\Psi}(x, y, z, t) = (f_1 u_0, f_2 v_0), \tag{4.15}$$

$$w(x, y, z, t) = -\nabla \cdot \boldsymbol{\Psi} = -f_{1_x} u_0 - f_1 u_{0_x} - f_2 v_{0_y}, \tag{4.16}$$

where f_1 and f_2 are defined in equations (3.2) and (3.3).

The relation to the free-surface location is provided by the linear kinematic free-surface condition:

$$\zeta_t(x, y, z, t) = w \,|_{z=0} = -u_{0_x} - v_{0_y}. \tag{4.17}$$

The bottom boundary condition, $w + \nabla \cdot \mathbf{u} = 0$, is satisfied in this representation.

Next, the horizontal component of the linearised momentum equation is utilised:

$$\rho w_t = -p_z - \rho g, \tag{4.18}$$

and by substituting the vertical velocity profile, we derive

$$p_z = \rho \left(f_{1_x} u_{0_t} + f_1 u_{0_{xt}} + f_2 v_{0_{yt}} - g \right). \tag{4.19}$$

https://doi.org/10.1017/jfm.2025.303 Published online by Cambridge University Press

The equation is vertically integrated from an arbitrary elevation z to the free surface while retaining only the leading-order terms:

$$p\,|_z^\zeta = p_a - p(x,\,y,\,z) = \rho\left(\left(\int_z^0 f_{1_x}\mathrm{d}z\right)u_{0_t} + \left(\int_z^0 f_1\mathrm{d}z\right)u_{0_{xt}} + \left(\int_z^0 f_2\mathrm{d}z\right)v_{0_{yt}} - g(\zeta - z)\right), \tag{4.20}$$

after which the pressure is isolated:

$$p = p_a + \rho\left(g(\zeta - z) - \left(\int_z^0 f_{1_x}\mathrm{d}z\right)u_{0_t} - \left(\int_z^0 f_1\mathrm{d}z\right)u_{0_{xt}} - \left(\int_z^0 f_2\mathrm{d}z\right)v_{0_{yt}}\right). \tag{4.21}$$

Taking the derivatives in the horizontal directions:

$$p_x = \rho\left(g\zeta_x - \left(\int_z^0 f_{1_{xx}}\mathrm{d}z\right)u_{0_t} - 2\left(\int_z^0 f_{1_x}\mathrm{d}z\right)u_{0_{xt}} - \left(\int_z^0 f_1\mathrm{d}z\right)u_{0_{xxt}} - \left(\int_z^0 f_{2_x}\mathrm{d}z\right)v_{0_{yt}} - \left(\int_z^0 f_2\mathrm{d}z\right)v_{0_{xyt}}\right), \tag{4.22}$$

$$p_y = \rho\left(g\zeta_y - \left(\int_z^0 f_{1_x}\mathrm{d}z\right)u_{0_{yt}} - \left(\int_z^0 f_1\mathrm{d}z\right)u_{0_{xyt}} - \left(\int_z^0 f_2\mathrm{d}z\right)v_{0_{yyt}}\right). \tag{4.23}$$

Defining $g_1 = \int_z^0 f_1\,\mathrm{d}z$, $g_2 = \int_z^0 f_2\,\mathrm{d}z$ and utilising the Leibniz integration rule:

$$p_y = \rho\left(g\zeta_y - g_{1_x}u_{0_{yt}} - g_1u_{0_{xyt}} - g_2v_{0_{yyt}}\right), \tag{4.24}$$

$$p_x = \rho\left(g\zeta_x - g_{1_{xx}}u_{0_t} - 2g_{1_x}u_{0_{xt}} - g_1u_{0_{xxt}} - g_{2_x}v_{0_{yt}} - g_2v_{0_{xyt}}\right). \tag{4.25}$$

These expressions are now substituted into the horizontal components of the momentum equation, applied in a vertically averaged sense:

$$F_1u_{0_t} = -gh\zeta_x + G_{1c}u_{0_t} + 2G_{1b}u_{0_{xt}} + G_{1a}u_{0_{xxt}} + G_{2b}v_{0_{yt}} + G_{2a}v_{0_{xyt}}, \tag{4.26}$$

$$F_2v_{0_t} = -gh\zeta_y + G_{1b}u_{0_{yt}} + 2G_{1a}u_{0_{xyt}} + G_{2a}v_{0_{yyt}}, \tag{4.27}$$

where $F_1 = \int_{-h}^0 f_{1_z}\mathrm{d}z$, $F_2 = \int_{-h}^0 f_{2_z}\mathrm{d}z$, $G_{1a} = \int_{-h}^0 g_1\mathrm{d}z$, $G_{1b} = \int_{-h}^0 g_{1_x}\mathrm{d}z$, $G_{1c} = \int_{-h}^0 g_{1_{xx}}\mathrm{d}z$, $G_{2a} = \int_{-h}^0 g_2\mathrm{d}z$ and $G_{2b} = \int_{-h}^0 g_{2_x}\mathrm{d}z$.

Equations (4.17), (4.26) and (4.27) provide a system of partial differential equations that can be solved for the vector stream function components and free-surface location. The equations are rotated to the fixed x, y axis system in the same way as in the 3-D PCSSE.

5. Simulations

Numerical simulations of the LPCSSE and the LTDPCE are compared with those of the ESWE, as these equations provide a first-order long-wave approximation. Additionally, the PCSSE derived by Schwartz *et al.* (2023) was simulated, with no visible differences observed compared with the LPCSSE in the examples and regions considered in the presented simulations. The simulations are achieved by numerically calculating the coefficients and using the NDsolve function in Mathematica. All simulations are time-harmonic, ensuring no additional treatment is needed for the time-dependent models.

https://doi.org/10.1017/jfm.2025.303 Published online by Cambridge University Press

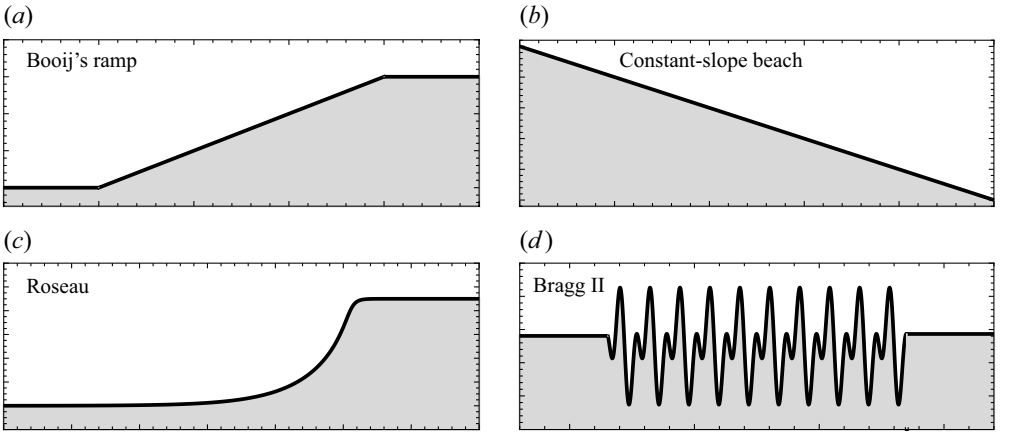

Figure 4. Illustration of the test case bathymetries.

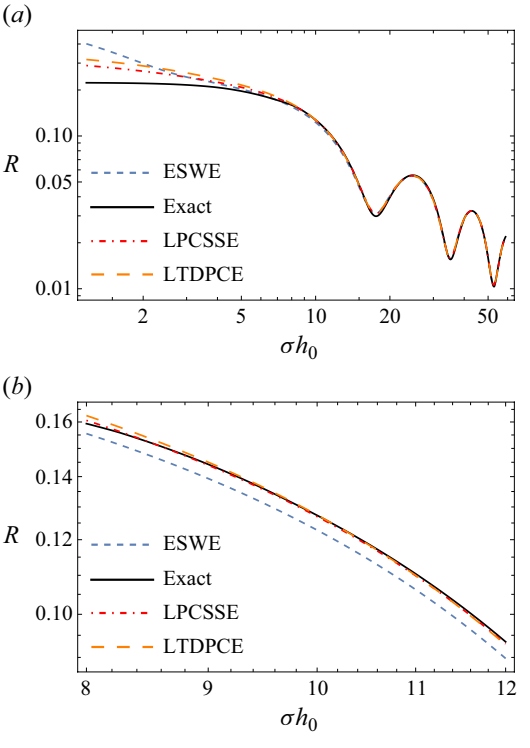

Figure 5. Reflection coefficient for a progressive wave flowing over Booij's ramp. (*a*) The full domain. (*b*) Enlargement of a part of the region.

The spatial step size is approximately 0.01. They are conducted on several bottom topographies (figure 4), including Booij's ramp, a constant-slope beach with normal and oblique incident waves, Roseau's bathymetry and a class II Bragg resonance. The results are presented in the following figures.

The bed shape in the form of a ramp, as tested by Booij (1983), is simulated in figure 5. The ramp consists of a constant-slope region between two semi-infinite horizontal

https://doi.org/10.1017/jfm.2025.303 Published online by Cambridge University Press

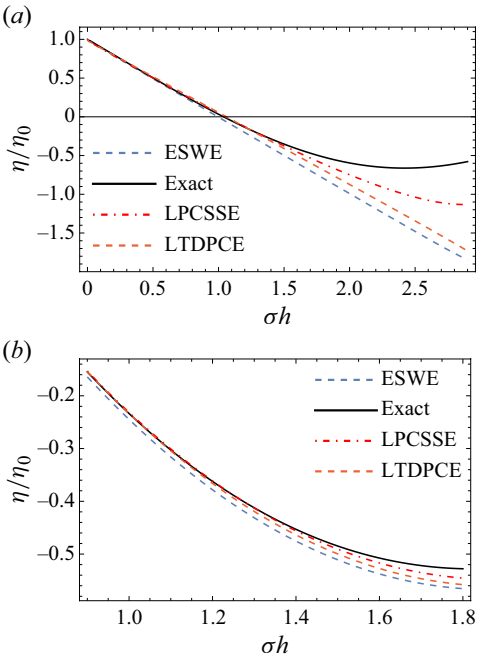

Figure 6. Normalised free-surface values versus σh for a normal incidence simulation. Regular standing wave with (*a*) 45° bed slope and (*b*) 30° bed slope.

segments. Both PC models provide a better match to the exact solution in the range σh_0 between 8 and 15 as shown in figure 5(*b*), as well as for waves shorter than $\sigma h_0 = 4$. For longer waves, the differences become indistinguishable.

The next test case involves normal and oblique incident waves on a constant-slope beach. An exact solution for waves that are normally incident to the bottom gradient is found in Stoker (1957) for bottom slopes of $\Pi/2n$, where n is an integer. A propagating wave solution is given as the sum of two standing waves: a regular standing wave, finite at the origin, and a singular standing wave, infinite at the origin. Simulations of the regular standing wave were performed on bed slopes up to 45°. A relative error $E_r = (R_m - R_a)/(R_a)$ is defined, where R_m and R_a are the PCMSE/ESWE model and the analytical reflection coefficients, respectively. For 45° degrees (figure 6*a*) the LPCSSE provides a very accurate result up to $\sigma h_0 = 1.3$ ($E_r = 0.0015$), while the ESWE deviates from the exact solution well before that ($E_r = 0.17$ at $\sigma h_0 = 1.3$). The LTDPCE closely follows the LPCSSE until $\sigma h_0 = 1.2$, then remains between the LPCMSE and ESWE ($E_r = 0.025$ at $\sigma h_0 = 1.3$). For 30° degrees (figure 6*b*), the results are similar but less pronounced. The analytical LPCSSE was simulated in this case, requiring only App_1 (2.8) for the calculation, and produced results identical to the approximated analytical equation.

Ehrenmark (1998) presented an exact solution for obliquely incident waves over a plane beach. The solution is limited, as in the normal incidence of Stoker, to bottom slopes of $\Pi/2n$, where n is an integer. Figure 7 shows the case of 45° oblique incidence on a 45° bottom slope. The ESWE model performs better up to $\sigma h = 1.2$ (maximum error of 0.034 for LPCMSE, 0.056 for LTDPCE and 0.007 for ESWE), but beyond that, the PC equations provide more accurate results (for example, at $\sigma h = 1.5$, the relative error is 0.064 for LPCMSE, 0.011 for LTDPCE and 0.18 for ESWE).

https://doi.org/10.1017/jfm.2025.303 Published online by Cambridge University Press

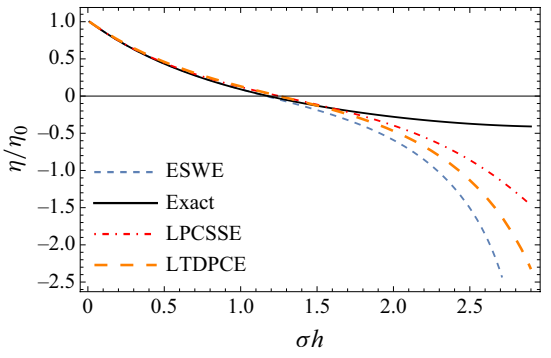

Figure 7. Normalised free-surface values versus σh for an oblique incidence simulation and an incidence angle of 45°.

Roseau (1976) derived the only analytical solution for waves propagating over a non-constant-slope bathymetry. In his solution, the bed location is defined by

$$\frac{x(\xi)}{h_0} = \xi - (2\Pi\beta)^{-1}\left(1 - \frac{h_L}{h_0}\right)\ln\left(1 + \mathrm{e}^{2\beta\Pi\xi} + 2\mathrm{e}^{\beta\Pi\xi}\cos(\beta\Pi)\right), \tag{5.1}$$

$$\frac{z(\xi)}{h_0} = -1 + (\Pi\beta)^{-1}\left(1 - \frac{h_L}{h_0}\right)\arctan\left(\frac{\sin(\beta\Pi)}{\mathrm{e}^{-\beta\Pi\xi} + \cos(\beta\Pi)}\right), \tag{5.2}$$

where $\beta \in (0, 1)$ is a shoaling parameter and the bed is defined parametrically as $z(\xi) = -h(x(\xi))$. The bed function tends to two flat semi-infinite sections at the limits $x \to \pm\infty$. In figure 8, a comparison of the reflection coefficients for the steepness value $\beta = 0.5$ is presented. The LPCSSE provides a significantly better match than the ESWE up to approximately $\sigma h_0 = 1.2$. The LTDPCE is even better, with results very close to the exact solution up to $\sigma h_0 = 1.6$. This is the region where the long-wave equations are expected to perform. The relative error of the reflection coefficients is presented in figure 8(*b*). For more moderate slopes, i.e. for smaller β values, the errors of all models reduce significantly.

The classical MSE, which accounts for second-order terms, generally provides a good agreement with the class I Bragg resonance. This phenomenon involves the interaction of two surface waves and one bottom undulation that satisfy predefined conditions (see e.g. Liu & Yue 1998). This is not the case in class II, for which they fail to provide a reasonable approximation. Class II involves the interaction of two surface waves and two bottom undulations. A simulation of the impact of class II on the free-surface values is provided in figure 9. This test case was presented by Guazelli *et al.* (1992) and involves two bed wavenumbers, $k_{b_1} = \pi/6\ \mathrm{cm}^{-1}$ and $k_{b_2} = \pi/3\ \mathrm{cm}^{-1}$, a patch length of $L = 48$ cm outside of which the bed is horizontal and a ratio of the average bottom depth to the bed wavenumber amplitude of $\Delta H/H_0 = 0.25$ and $H_0 = 2.5$ cm. Guazelli's model, which is used for the comparison, accounts for three evanescent modes. In the first peak ($\sigma h \approx 1.7$), the PC-based models show a significantly better match than the ESWE compared with the numerical results of Guazelli. This peak is the result of the class II resonance. In the second peak ($\sigma h \approx 3.1$), the LTDPCE and ESWE are very far off. The LPCSSE shows a reasonable match with the peak location and an excellent match with the width and maximum value of the peak curve. This peak is the result of class I resonance.

https://doi.org/10.1017/jfm.2025.303 Published online by Cambridge University Press

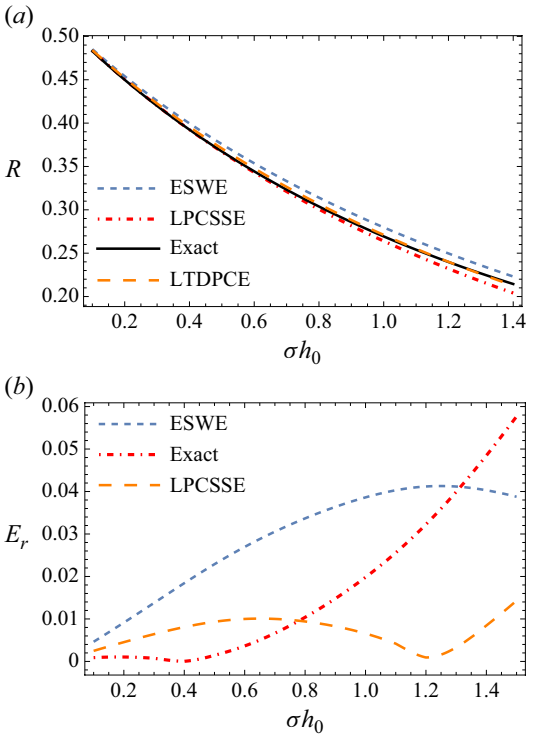

Figure 8. (*a*) Simulation of the reflection coefficient versus σh_0 for the Roseau bathymetry; $\beta = 0.5$, $h_L/h_0 = 0.1$. (*b*) Simulation of the relative error versus σh_0.

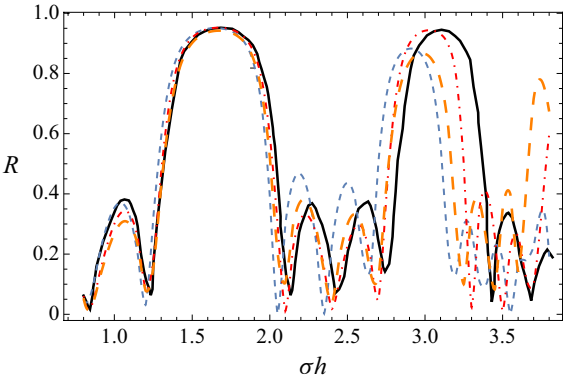

Figure 9. Comparison of the reflection coefficient values obtained from simulations of the LPCSSE (red dot-dashed curve), ESWE (blue small-dashed curve), LPCTDE (orange large-dashed curve) and the experimental results obtained by Guazzelli, Rey & Belzons (1992) as shown in figure 2 of that article (black solid curve).

6. Conclusions

The formulation of a 2-D long-wave PCSSE is outlined. Unlike the full PCSSE, an approximate, explicit expression of the coefficients in the equation is developed, with no limitations on the steepness of the bed. This is achieved by approximating the tanh function as a finite polynomial. Due to this simplification, the vertical profile of the flow parameters is simplified, allowing for analytical vertical integration. Following this, an extension of

https://doi.org/10.1017/jfm.2025.303 Published online by Cambridge University Press

the quasi-3-D equation for obliquely incident waves to a full 3-D equation is formulated. A local axis system is defined, with one axis pointing in the depth gradient direction, resulting in a locally horizontal bottom in the perpendicular direction. After deriving an equation in the dynamic axis system, the equation is rotated to the fixed axis system, where the axes are parallel and perpendicular to the beach. This general case was absent in the development of the original equation and is an important contribution to its application. The equations stated thus far are developed using a time-averaged variational approach in the frequency domain. Corresponding 2-D and 3-D equations in the time domain are also developed.

The LPCSSE and LTDPCE were compared with the ESWE for several 2-D test cases, in addition to the quasi-3-D case of obliquely incident waves. The PC-based equations provide a better match to the analytical results in almost all of the simulations. The differences were more pronounced for steeper bottom slopes. These results demonstrate the advantage of a PC-based equation over an equivalent Cartesian-based equation in the long-wave region.

Declaration of interests. The author reports no conflict of interest.

References

BELIBASSAKIS, K.A. & ATHANASSOULIS, G.A. 2006 A coupled mode technique for the run-up of non-breaking dispersive waves on plane beaches. In Proc. 25th Int.Conf. on Offshore Mechanics and Arctic Engineering, OMAE2006. American Society of Mechanical Engineers (ASME).

BERKHOFF, J.C.W. 1972 Computation of combined refraction-diffraction. In The 13th International Conference on Coastal Engineering, pp. 471–490. American Society of Civil Engineers (ASCE).

BOOIJ, N. 1983 A note on the accuracy of the mild-slope equation. *Coast. Engng* **7** (3), 191–203.

CHAMBERLAIN, P.G. & PORTER, D. 1995 The modified mild slope equation. *J. Fluid Mech.* **291**, 393–407.

EHRENMARK, U.T. 1998 Oblique wave incidence on a plane beach: the classical problem revisited. *J. Fluid Mech.* **368**, 291–319.

GUAZZELLI, E., REY, V. & BELZONS, M. 1992 Higher-order Bragg reflection of gravity surface waves by periodic beds. *J. Fluid Mech.* **245**, 301–317.

HASTINGS, C. 1955 *Approximations for Digital Computers*. Princeton University Press.

KIM, J.W. & BAI, K.J. 2004 A new complementary mild slope equation. *J. Fluid Mech.* **511**, 25–40.

KIRBY, J.T. 1986 A general wave equation for waves over rippled beds. *J. Fluid Mech.* **162**, 171–186.

LIU, Y. & YUE, D.K.P. 1998 On generalized Bragg scattering of surface waves by bottom ripples. *J. Fluid Mech.* **356**, 297–326.

MILES, J.W. & CHAMBERLAIN, P.G. 1998 Topographical scattering by gravity waves. *J. Fluid Mech.* **361**, 175–188.

PORTER, R. 2019 An extended linear shallow water equation. *J. Fluid Mech.* **876**, 413–427.

ROSEAU, M. 1976 *Asymptotic Wave Theory*. Amsterdam- Oxford.

SCHWARTZ, R., ORON, A. & AGNON, Y. 2023 The polar-Cartesian mild-slope equation. *J. Fluid Mech.* **970** (A4), 1–22.

SMITH, R. & SPRINKS, T. 1975 Scattering of surface waves by a conical island. *J. Fluid Mech.* **72** (02), 373–384.

STOKER, J.J. 1957 *Water Waves*. Interscience.

TOLEDO, Y. & AGNON, Y. 2010 A scalar form of the complementary mild-slope equation. *J. Fluid Mech.* **656**, 407–416.

https://doi.org/10.1017/jfm.2025.303 Published online by Cambridge University Press